NASA/TM—2001-210567

Supersonic Wind Tunnel Tests of a Half-Axisymmetric 12°-Spike Inlet to a Rocket-Based Combined-Cycle Propulsion System

J.R. DeBonis and C.J. Trefny
Glenn Research Center, Cleveland, Ohio

Prepared for the
37th Combustion Subcommittee, 25th Airbreathing Propulsion Subcommittee,
and 19th Propulsion Systems Hazards Subcommittee Joint Meeting
sponsored by the Joint Army-Navy-Air Force Interagency Propulsion Committee
Monterey, California, November 13–17, 2000

National Aeronautics and
Space Administration

Glenn Research Center

February 2001

Available from

NASA Center for Aerospace Information
7121 Standard Drive
Hanover, MD 21076
Price Code: A03

National Technical Information Service
5285 Port Royal Road
Springfield, VA 22100
Price Code: A03

Available electronically at http://gltrs.grc.nasa.gov/GLTRS

SUPERSONIC WIND TUNNEL TESTS OF A HALF-AXISYMMETRIC 12°-SPIKE INLET TO A ROCKET-BASED COMBINED-CYCLE PROPULSION SYSTEM

J.R. DeBonis and C.J. Trefny
National Aeronautics and Space Administration
Glenn Research Center
Cleveland, Ohio 44135

SUMMARY

Results of an isolated inlet test for NASA's GTX air-breathing launch vehicle concept are presented. The GTX is a Vertical Take-off/Horizontal Landing reusable single-stage-to-orbit system powered by a rocket-based combined-cycle propulsion system. Tests were conducted in the NASA Glenn 1- by 1-Foot Supersonic Wind Tunnel during two entries in October 1998 and February 1999. Tests were run from Mach 2.8 to 6. Integrated performance parameters and static pressure distributions are reported. The maximum contraction ratios achieved in the tests were lower than predicted by axisymmetric Reynolds-averaged Navier-Stokes computational fluid dynamics (CFD). At Mach 6, the maximum contraction ratio was roughly one-half of the CFD value of 16. The addition of either boundary-layer trip strips or vortex generators had a negligible effect on the maximum contraction ratio. A shock boundary-layer interaction was also evident on the end-walls that terminate the annular flowpath cross section. Cut-back end-walls, designed to reduce the boundary-layer growth upstream of the shock and minimize the interaction, also had negligible effect on the maximum contraction ratio. Both the excessive turning of low-momentum corner flows and local over-contraction due to asymmetric end-walls were identified as possible reasons for the discrepancy between the CFD predictions and the experiment. It is recommended that the centerbody spike and throat angles be reduced in order to lessen the induced pressure rise. The addition of a step on the cowl surface, and planar end-walls more closely approximating a plane of symmetry are also recommended. Provisions for end-wall boundary-layer bleed should be incorporated.

SYMBOLS

A	area
CRG	geometric contraction ratio
M	Mach number
P	pressure
Re	Reynolds number
R	recovery
r	radial coordinate
T	temperature
x	axial coordinate
Δx	centerbody translation

Subscripts

1	spike tip location
2	throat location
arc	circular arc
avg	averaged quantity
c	capture
cav	continuity averaged quantity
cb	centerbody
cl	cowl
t	total condition

INTRODUCTION

One of the three primary goals of NASA's Aeronautics and Space Transportation Technology Program is to enable low-cost access to space by developing advanced space transportation concepts and technologies. The key to reducing space launch costs is developing a reusable vehicle with a short turnaround time. Highly reusable implies a very robust single-stage-to-orbit (SSTO) vehicle. NASA Glenn Research Center has undertaken a program to demonstrate such a vehicle. The concept, called the GTX[1] (formerly Trailblazer) (Figure 1), is powered by a rocket-based combined-cycle (RBCC) engine (Figure 2). This engine is designed to operate efficiently from lift-off to orbit by integrating a rocket and ramjet.[2] The system combines the high thrust-to-weight characteristics of a rocket with the high specific impulse characteristics of a ramjet. The air-breathing propulsion system reduces the propellant fraction required for an SSTO vehicle from that of a rocket and thus enables the robust structure required for reusable operation. Ultimately, the feasibility and cost of this SSTO system will depend on vehicle weight and complexity. Therefore, structural efficiency and minimum complexity must be considered during development of all aspects of the vehicle.

The engines are housed in three semicircular engine pods located near the aft portion of the vehicle. The pods allow for diversion of the boundary layer, simplify centerbody actuation and sealing, and enable integration of the nozzles with the vehicle base. The engine operates in air-breathing modes from lift-off to between Mach 10 and 12, at which point the air-breathing engine flow path is closed off, and the rocket is turned back on to carry the vehicle out of the atmosphere and into orbit. An important component of the RBCC engine is the inlet. This device must efficiently capture and compress air over the entire range of air-breathing Mach numbers. The configuration is semi-axisymmetric (a sector of an annular inlet) to take advantage of the inherent structural efficiency. The inlet axis of symmetry lies on a cylindrical reference surface that also defines the end-walls of the annular sector (as such, the end-walls are not planes of symmetry). The cylindrical reference surface is concentric with and lies outside the axisymmetric vehicle forebody to accommodate diversion of the forebody boundary layer.

The inlet reported on is designated as the 6g configuration.[3] The centerbody, the engine's only moving part, translates axially to vary the contraction ratio over the Mach number range and allows the inlet to start. Completely retracting the centerbody closes off the inlet duct for rocket operation in a vacuum. Because the GTX vehicle continuously accelerates through the atmosphere, the cruise condition that is typically used as a basis for design does not exist. Since the required inlet contraction ratio (the ratio of the area of the captured stream tube to the throat area) and shock angle both do not change appreciably beyond Mach 6, this flight condition was used as the design basis. Isentropic mixed compression inlet contours were generated using the method of characteristics. The inlet centerbody had a cone half-angle of 12°. This angle was chosen to keep the length and, hence, weight of the centerbody to a minimum. At Mach 6 the centerbody shock is on the cowl lip at a contraction ratio of 16. The shoulder on the centerbody was positioned to cancel the reflected cowl shock. At the throat, the walls are angled at 15° toward the axis to minimize length. A back step in the centerbody is located here to isolate the forward portion of the inlet from backpressure feeding forward through the subsonic portion of the boundary layer and also serves as a location for fuel injection.

Several perfect gas Reynolds-averaged Navier-Stokes (RANS) computational fluid dynamics (CFD) analyses using the NPARC code[4] were done on preliminary configurations. The CFD solutions were used to evaluate the designs and provide guidance in adjusting key geometric parameters. The final 6g inlet contours and key parameters are pictured in Figure 3. The geometry is completely described in Table 1. The contours are defined with the centerbody spike in the fully closed (aft) position. A plot of the inlet's area distribution for several spike positions is shown in Figure 4. The cowl lip radius (r_{cl}) for the full-scale vehicle is 33.1 in. (84.1 cm). Key locations in the flowpath are numbered for easy reference (Figure 2). Station 0 is the free-stream. Station 1 is located at the inlet spike tip and represents the conditions after the flow is processed by the vehicle forebody. Station 2 is at the inlet throat, and station 3 is at the end of the hub.

The objectives of the test program reported herein were to determine the operability and performance of the 6g configuration, provide data for design refinements, and validate design and prediction methods.

APPARATUS AND PROCEDURE

An 8-percent scale model of the GTX 6g inlet, with translating centerbody, was built for subscale testing. The model included the boundary-layer diverter and was placed on a rocket body fairing. The rocket body fairing provides a pressure boundary surface for the conical centerbody shock. It is not intended for boundary-layer simu-

tion. The model was designed to approximate the flowfield provided to the cowl lip plane in the full-scale vehicle. Pictures of the inlet model are shown in Figure 5.

A remote hydraulic actuator translated the centerbody. A linear voltage differential transducer (LVDT) sensed the position of the spike. Prior to each test run, the LVDT was calibrated to spike position. Throat area was determined as a function of spike position prior to model installation using a series of ball gauges.

A cold-pipe and mass-flow plug assembly was used to mimic the effects of combustion by providing backpressure to the inlet. The cold pipe is a 12-in.- (30.48-cm-) long, 3.25-in.- (8.255-cm-) diameter tube with four static pressure taps located circumferentially 1 diameter upstream of the exit. The mass-flow plug, located at the aft end of the cold pipe, is a 16.5° half-angle cone with a spherical nose. The plug was translated with a hydraulic actuator to vary the choked exit area of the cold pipe, and its position was measured with an LVDT. A mass-flow measurement is obtained from the cold-pipe static pressure, tunnel total temperature, and choked plug area. The mass-flow plug was calibrated prior to installation of the inlet model using three pitot inlets of varying diameters, which provide a known mass flow to the cold pipe.

The model was instrumented with 136 static pressure taps. Five axial rows of taps were located on both the cowl and centerbody, at angles of 0°, ±39°, and ±79° with respect to the plane of symmetry. Additional taps were located on the inlet end-walls, centerbody hub, and rocket body fairing. Five total pressure rakes, each with five pitot probes, were placed at the trailing edge of the hub at 0°, ±39°, and ±79°. The probes on each rake were located on centers of equal area.

The test was conducted in the NASA Glenn Research Center's 1- by 1-Foot Supersonic Wind Tunnel[5] (1×1 SWT). It is a continuous flow aerodynamic facility that is capable of producing discrete Mach numbers between 1.3 and 6.0. Mach number variation is achieved by replacing the nozzle section of the tunnel. A separate nozzle block is used for each Mach number. At Mach 5 and 6, an electric heater in parallel with the plenum chamber is used to heat the air to prevent oxygen liquefaction of the flow. The model was installed on the sidewall of the test section. A schlieren video system was used to visualize the shock patterns external to the inlet and aided in determining when the inlet unstarted. The tests were run at the facility's maximum Reynolds number at each Mach number. Tunnel conditions for the inlet test are listed in Table 2.

Test Procedure

The inlet centerbody was translated fully forward during tunnel startup to ensure that the inlet started. Once a steady condition was reached in the tunnel test section, the mass-flow plug position was set to ensure that the cold pipe exit was choked for an accurate mass-flow measurement. Contraction ratio sweeps were performed by translating the centerbody aft in small increments until the inlet unstarted. Once the maximum contraction ratio was determined, the centerbody positions corresponding to the 90- and 95-percent maximum contraction ratio were computed. The centerbody was set at these positions and backpressure sweeps were performed where the mass-flow plug was translated in small increments until the inlet unstarted due to backpressure.

Data Reduction

Data at the inlet throat (station 2) was obtained using a continuity averaging procedure. An average static pressure was computed from the pressure taps at this location. Then a continuity-averaged Mach number was computed using the total temperature of the flow, the average static pressure, the measured mass flow, and the throat area. Total pressure at the throat was computed using the continuity-averaged Mach number and the average static pressure.

RESULTS AND DISCUSSION

Two test entries in the 1×1 SWT were made, in October 1998 and February 1999. During the first entry, the inlet was tested at Mach 2.8, 3.0, 4.0, 5.0 and 6.0. A test at Mach 2.5 was attempted, but the tunnel did not start due to blockage. The inlet started at all the Mach numbers tested. Contraction ratio sweeps at all Mach numbers found that the maximum contraction ratio obtained was less than predicted by the axisymmetric CFD analyses. At Mach 6, the maximum contraction ratio was one-half the CFD predicted value of 16. For Mach 5 and 6, it was noted that the pressure distributions on the cowl and centerbody surfaces were symmetric about the centerline at low contraction ratios. However, as the contraction ratio was increased towards its maximum, the distributions became asymmetric and the pressures at the ±79° locations became larger than the 0° pressures.

The total pressure rakes at station 3 exhibited unsteady behavior under backpressure at 90 and 95 percent of the maximum contraction ratio, and revealed that the diffuser was separated. The limited contraction ratio obtained in the test resulted in high throat Mach numbers. The pressure rise behind the subsequent shock system was higher than intended and caused a separated boundary layer in the diffuser. No data from the total pressure rakes is presented.

An oil flow visualization run was made at Mach 4. Drops of oil were applied over the entire centerbody, in both diverter channels, and on the rocket body fairing. Once supersonic flow was established in the tunnel, the model was set to 90 percent of the maximum contraction ratio. This condition was held for 15 min and then the tunnel was quickly shut down. Good oil flow traces were obtained (Figure 6). These traces showed a symmetric circumferential separation on the centerbody caused by the reflected cowl shock. The oil flow also showed that this shock caused a shock wave boundary-layer interaction on the end-walls. Secondary flows in the corners were also evident on the end-walls.

It was thought that the separation on the centerbody was limiting the maximum contraction ratio and causing the discrepancy with the axisymmetric CFD. Two attempts were made to reduce the separation and increase the maximum contraction ratio. First, grit was applied on the centerbody to ensure that the boundary layer would be turbulent and less susceptible to separation. For Mach 2.8, 3.0, and 4.0, a 0.25-in.- (0.635-cm-) wide strip of no. 80 grit was placed 3.5 in. (8.89 cm) downstream of the spike tip. For Mach 5.0 and 6.0, a 0.25-in.- (0.635-cm-) wide strip of no. 36 grit was placed 5 in. (12.7 cm) downstream of the spike tip. The grit had no effect on the maximum contraction ratio, indicating that the boundary layer was turbulent.

Second, vortex generators were placed on the centerbody 1.5 in. (3.81 cm) upstream of the cowl shock reflection point to energize the boundary layer prior to the shock boundary-layer interaction. The vortex generators consisted of 0.25-in.- (0.635-cm-) steel strapping material spot welded to the centerbody surface. Twenty vortex generators were equally spaced circumferentially around the spike (approximately 0.35 in. (0.889 cm) apart). They were 0.050 in. (0.127 cm) high and angled at 5° to the freestream flow (Figure 7). The vortex generators also had no effect, indicating either that the contraction-ratio-limiting phenomenon was associated with the end-walls, or that the vortex generators did not overcome excessive turning and shock pressure rise.

The second tunnel entry was made to investigate the effect of end-wall leading edge modifications on the maximum contraction ratio. Interchangeable end-wall leading edges were used to try to affect the reflected cowl shock boundary-layer interaction on the end-wall. Four angles of leading edge sweep (measured normal to the inlet axis) were tested: 60° swept forward, 0° (no sweep), 60° swept aft, and 75° swept aft (Figure 8). The aft swept leading edges were intended to minimize boundary-layer buildup on the end-walls upstream of the cowl shock and reduce the shock wave boundary-layer interaction. The 60° sweep-back angle ensures that the cowl shock is behind the end-wall leading edge for all Mach numbers tested. The 75° sweep-back angle ensures that the cowl shock is behind the leading edge above Mach 4. Contraction ratio sweeps were made with the 0°, 60° swept aft, and 75° swept aft end-wall configurations. No significant effect on the maximum contraction ratio was found, indicating that the shock wave boundary-layer interaction on the end-wall was not limiting the contraction ratio. Also, the asymmetry in the pressure distributions was still present at high contraction ratios.

Several possible causes remain for the limited contraction ratio as compared to the CFD predictions. The CFD assumed the flow was axisymmetric and neglected the effect of the end-walls. The end-wall surface is cylindrical and does not form a plane of symmetry. In effect, this nonaxisymmetric geometry increases the contraction in the vicinity of the end-walls. Low momentum flow in the corners, in combination with the aggressive turning in the design, may also be the limiting factor.

A complete set of contraction ratio and backpressure sweeps using the 60° aft swept end-walls were made at all Mach numbers, and that data is reported herein. Mass capture is plotted versus geometric contraction ratio in Figure 9. Mass capture monotonically increases with contraction ratio at each Mach number as the spike is translated aft. Full mass capture is not achieved at Mach 6 because the inlet was designed to be shock-on-lip at a contraction ratio of 16, which was not achieved in the test. Throat pressure, throat Mach number, and throat recovery are shown in Figures 10, 11, and 12, respectively. The increase in recovery with contraction ratio at low Mach numbers and low contraction is attributed to the fact that the inlet is far off the design point and at increasing Mach numbers and contraction ratio approaches the design condition.

The discontinuous drop in the recovery and Mach number data can be attributed to the asymmetric pressure distributions at high contraction. The high pressures near the end-walls bias the average throat pressure measurement and result in low Mach numbers and recoveries. This bias in static pressure propagates into the Mach number calculation and its effect is magnified in the total pressure and recovery calculation because the square of the Mach number is used.

Pressure distributions on the cowl and centerbody centerlines at the last symmetric contraction ratio are presented in Figure 13. The lower curves represent the centerbody pressures and the upper curves represent the cowl pressures. Maximum backpressure ratios of 12.5, 15.5, 43, 83.5, and 158 were achieved for Mach 2.8, 3, 4, 5, and 6, respectively. No influence of backpressure on the upstream centerbody pressures was seen at low and moderate backpressure, indicating that the step in the centerbody serves as an effective isolator. At very high backpressure, the pressure feeds forward (possibly along the end-walls) and affects the upstream pressure distributions.

Figures 14 to 18 summarize the maximum performance of the inlet as a function of Mach number. Data for both the last started point and the last symmetric point for Mach 5 and 6 are presented. The maximum contraction ratio predicted by axisymmetric CFD is plotted for comparison in Figure 14. The mass-flow ratio predicted by a Taylor-Maccoll solution at the last started spike positions is plotted for reference in Figure 15.

SUMMARY AND CONCLUSIONS

A model of the GTX configuration 6g inlet was tested in the 1- by 1-Foot Supersonic Wind Tunnel (1×1 SWT) during two entries in October 1998 and February 1999. Isolated inlet tests were run from Mach 2.8 to 6. The tunnel would not start at Mach 2.5. The inlet is a sector of an axisymmetric, mixed-compression, translating centerbody configuration designed for shock-on-lip at Mach 6 at a contraction ratio of 16. The inlet started and contraction ratio sweeps were obtained at all Mach numbers tested. Backpressure sweeps were obtained for selected contraction ratios at each Mach number. A step in the centerbody contour at the throat acted as an effective isolator.

The maximum contraction ratio was less than that predicted by axisymmetric RANS calculations over the entire Mach number range tested. At Mach 6, the maximum contraction ratio was roughly one-half of the CFD value of 16. Under-prediction of the extent of centerbody boundary-layer separation was identified as a possible reason for the discrepancy. A grit strip was placed on the centerbody spike to ensure that the boundary layer approaching the cowl shock reflection point would be turbulent. This had no effect on the maximum contraction ratio, indicating that the centerbody boundary layer was already turbulent. A row of vortex generators placed on the spike to energize the boundary layer also had negligible effect. Oil flow visualization was done at Mach 4. Flow separation on the centerbody surface due to the reflected cowl shock was apparent. A shock boundary-layer interaction was also evident on the end-walls that terminate the annular flowpath cross section. During the second entry, cut-back end-walls were tested to minimize boundary-layer growth upstream of the glancing reflected cowl shock. End-walls were tested with leading edges normal to the inlet axis and swept back 60° and 75° from the cowl lip plane. None of these configurations resulted in a higher maximum contraction ratio than the original 60° swept-forward configuration tested during the first entry.

It is concluded that excessive turning of low-momentum corner flows and local over-contraction due to asymmetric end-walls limited the contraction ratio to a smaller number than predicted by the axisymmetric RANS calculations. It is therefore recommended that the spike and throat angles be reduced in order to lessen the pressure rise in the boundary layers and low-momentum corner flows. It is recommended that the end-wall surfaces be changed to axisymmetric planes of symmetry to eliminate the distortion at the throat caused by the cylindrical end-walls. Provisions for boundary-layer bleed should be incorporated into these new end-walls. Finally, a step comparable to that on the centerbody should be added to the cowl at the throat station.

REFERENCES

[1] Trefny, C.J., "An Air-Breathing Launch Vehicle Concept for Single-Stage-to-Orbit," AIAA Paper 99–2730, June 1999.

[2] Escher, W.J.D., "Synerjet for Earth/Orbit Propulsion: Revisiting the 1966 NASA/Marquardt Composite (Airbreathing/Rocket) Propulsion System Study," SAE Paper 851163, May 1985.

[3] DeBonis, J.R., Trefny, C.J., and Steffen Jr., C.J., "Inlet Development for a Rocket Based Combined Cycle, Single Stage to Orbit Vehicle Using Computational Fluid Dynamics," AIAA 99-2239, NASA/TM—1999-209279, June 1999.

[4] Power, G.D., Cooper, G.K., and Sirbaugh, J.R., "NPARC 2.2 – Features and Capabilities," AIAA Paper 95-2609, July 1995.

[5] Seablom, K.D., Soeder, R.H., Stark, D.E., Leone, J.F.X., and Henry, M.W., "NASA Glenn 1- by 1-Foot Supersonic Wind Tunnel User Manual," NASA/TM—1999-208478, April 1999

	x_{cl}/r_{cl}	r_{cl}/r_{cl}	A	B	C	D
Cowl lip	-2.8192	1.0000				
Begin spline 1	-2.4192	1.0000	1.3146E-01	6.1873E-01	6.8555E-01	8.9863E-01
Begin spline 2	-1.3600	0.7800	-5.2929E-03	8.7712E-02	-1.6807E-10	6.0445E-01
Station 3	0.0000	0.6045				

a. Cowl

	x_{cb}/r_{cl}	r_{cb}/r_{cl}				
Spike tip	-6.1164	0.0000				
			r_{arc}/r_{cl}	x_{arc}/r_{cl}	y_{arc}/r_{cl}	
Begin circular arc	-2.1040	0.8529	5.0000E-01	-2.0000E+00	3.6379E-01	
			A	B	C	D
Begin spline 3	-2.0000	0.8638	-1.4944E-02	-2.8465E-01	-9.5929E-01	-3.5726E-02
Begin spline 4	-1.3600	0.7498	1.1242E-01	4.8397E-01	3.7978E-01	6.5394E-01
Begin spline 5	-1.1100	0.6749	2.1372E-02	-2.6519E-03	-3.6397E-01	3.0342E-01
Centerbody trailing edge	0.0000	0.3034				

b. Centerbody

Splines defined by, $\frac{r}{r_{cl}} = A\left(\frac{x}{r_{cl}}\right)^3 + B\left(\frac{x}{r_{cl}}\right)^2 + C\frac{x}{r_{cl}} + D$

Table 1. Inlet geometry

Mach	P_t (psi)	T_t (R)	Test Re	Flight Re	Re Ratio
2.8	50	520	2.0E+06	10.2E+06	5.1
3.0	75	520	2.7E+06	9.7E+06	3.6
4.0	160	516	3.6E+06	7.2E+06	2.0
5.0	165	611	1.8E+06	5.8E+06	3.2
6.0	165	812	0.8E+06	4.7E+06	5.9

Test Re based on 2.65" cowl lip radius
Flight Re based on 33.1" cowl lip radius

Table 2. 1x1 SWT conditions

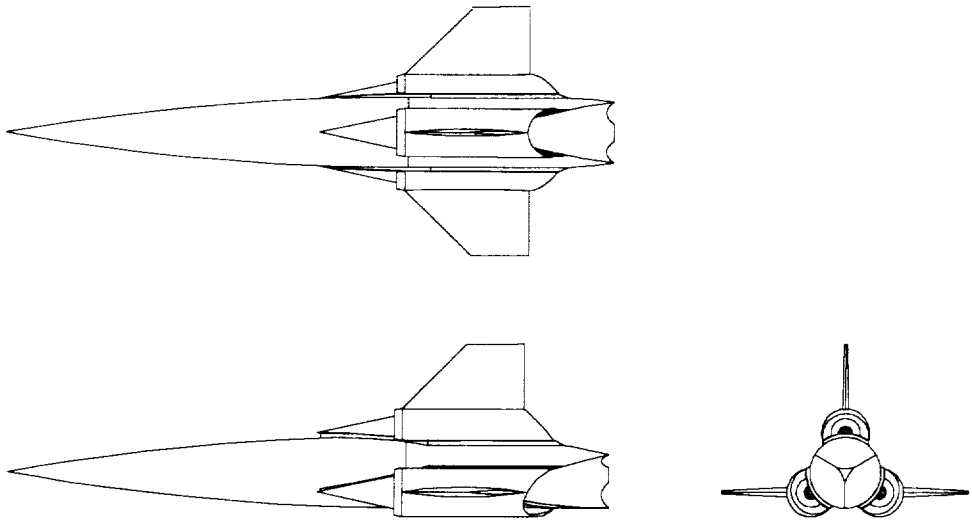

Figure 1. GTX vehicle

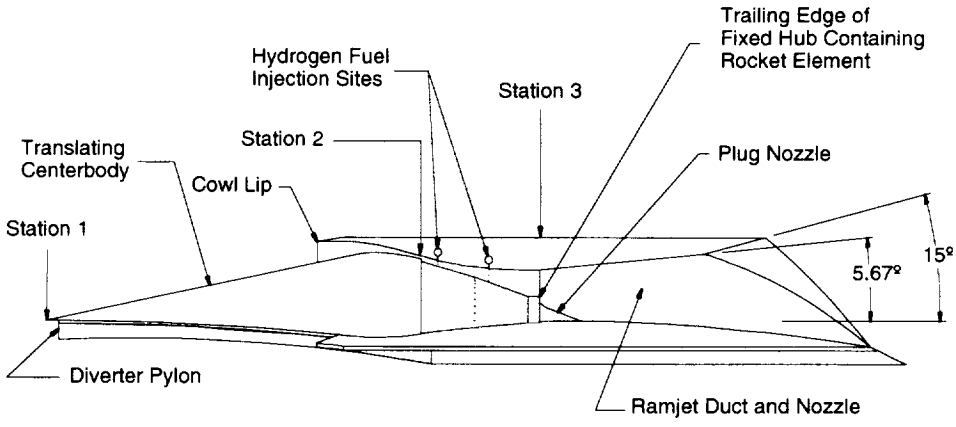

Figure 2. GTX RBCC engine

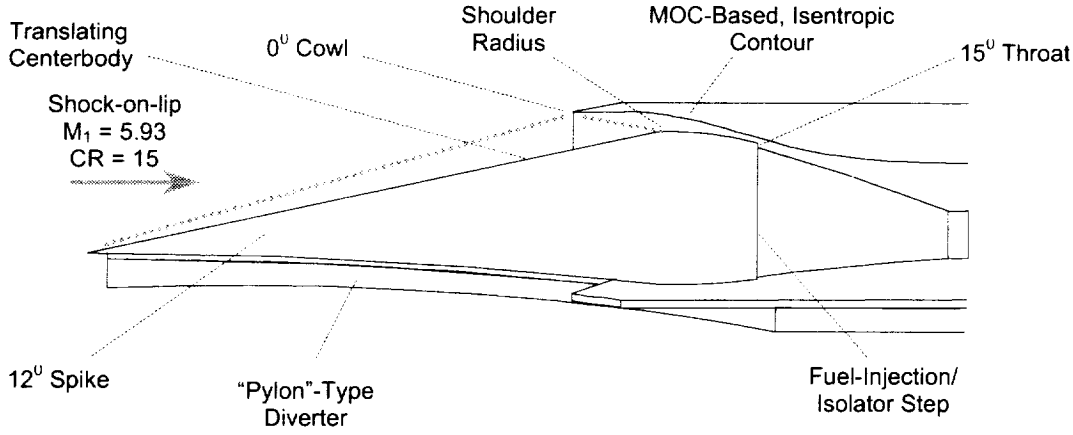

Figure 3. Inlet geometry definition

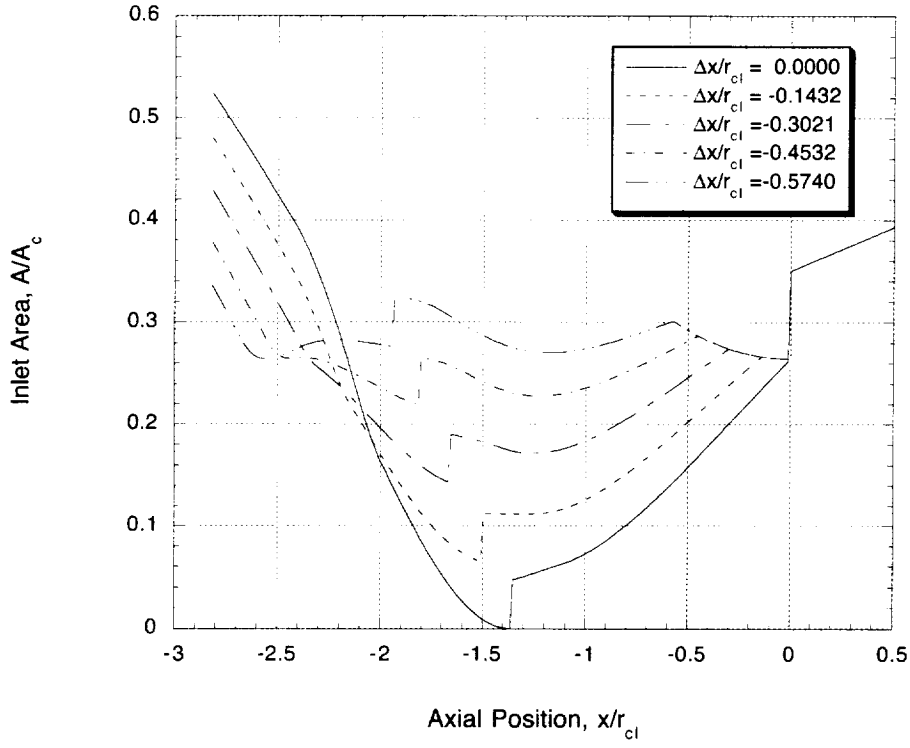

Figure 4. Inlet area distribution

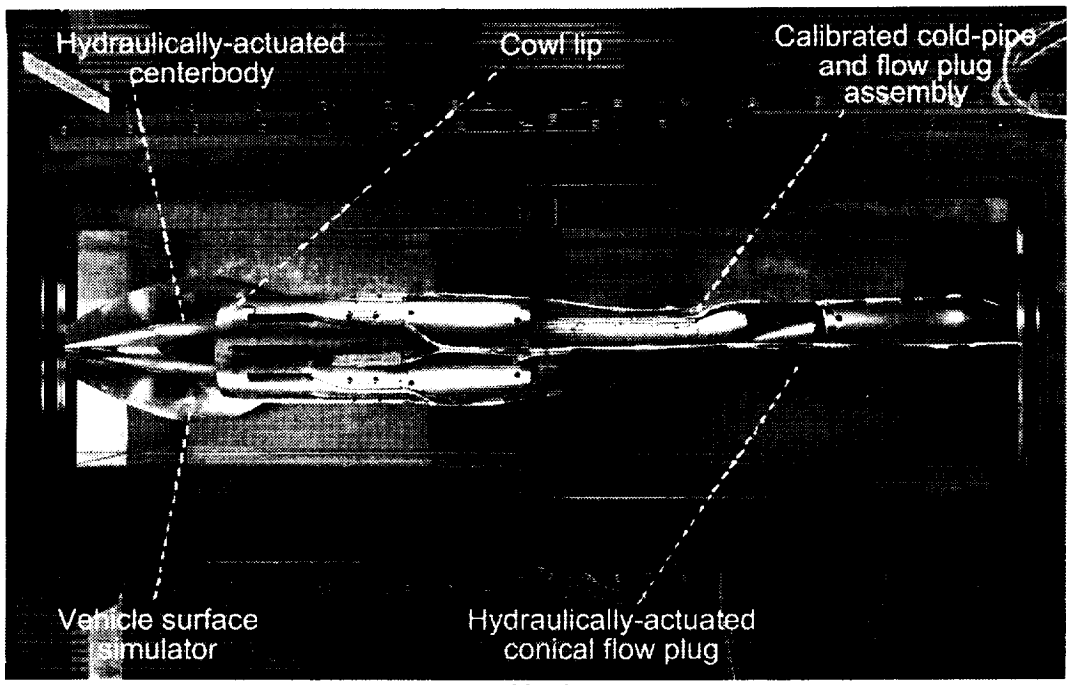

a. side view

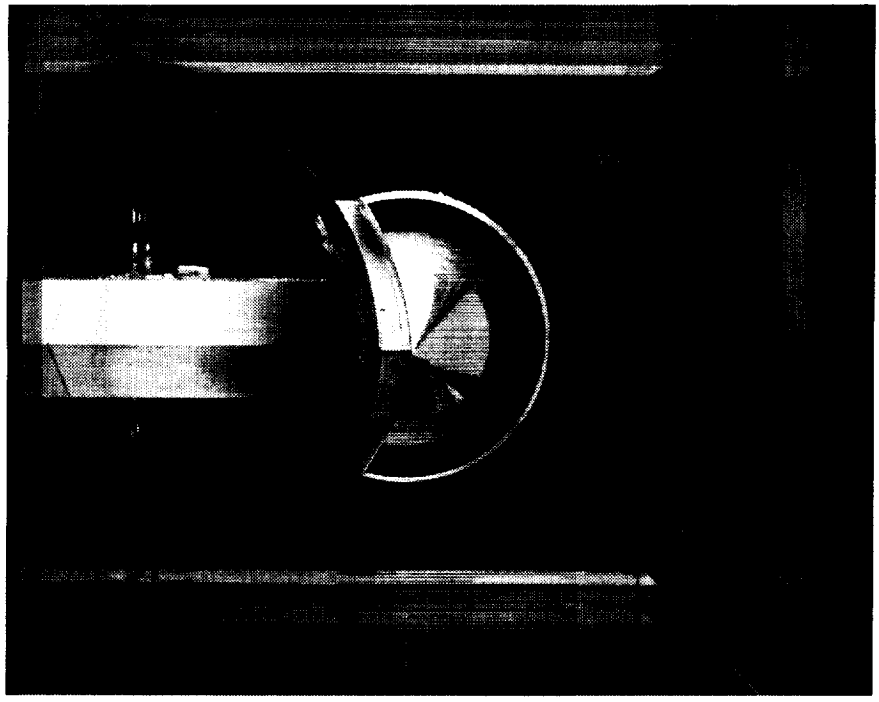

b. front view

Figure 5. Inlet model installed in 1x1 SWT

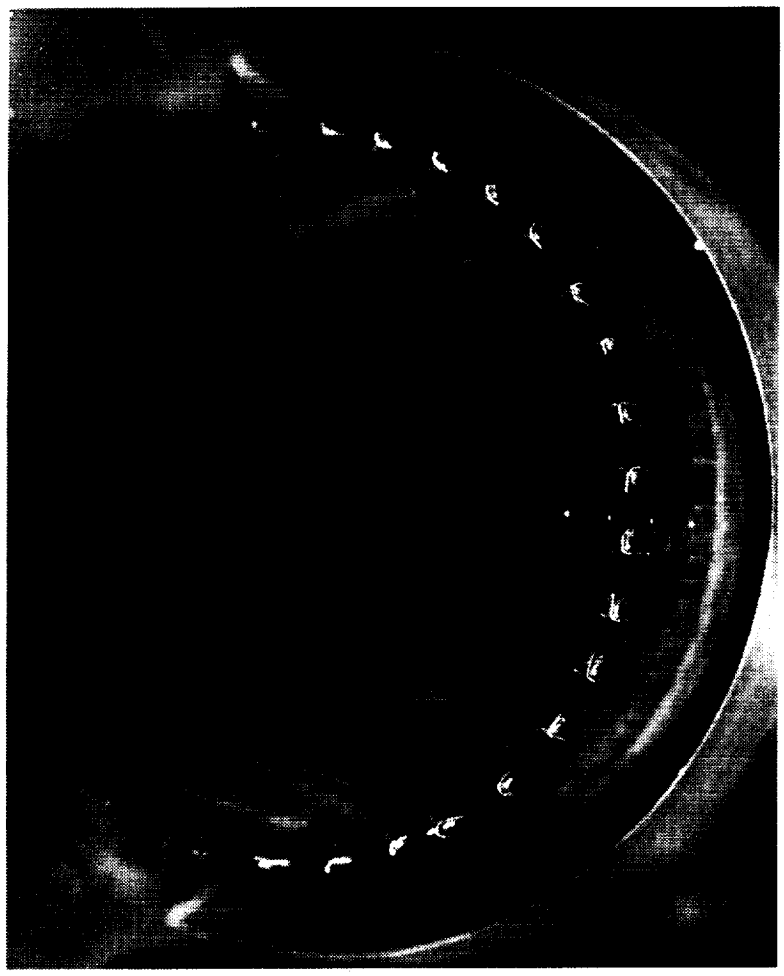

Figure 6. Vortex generators installed on centerbody

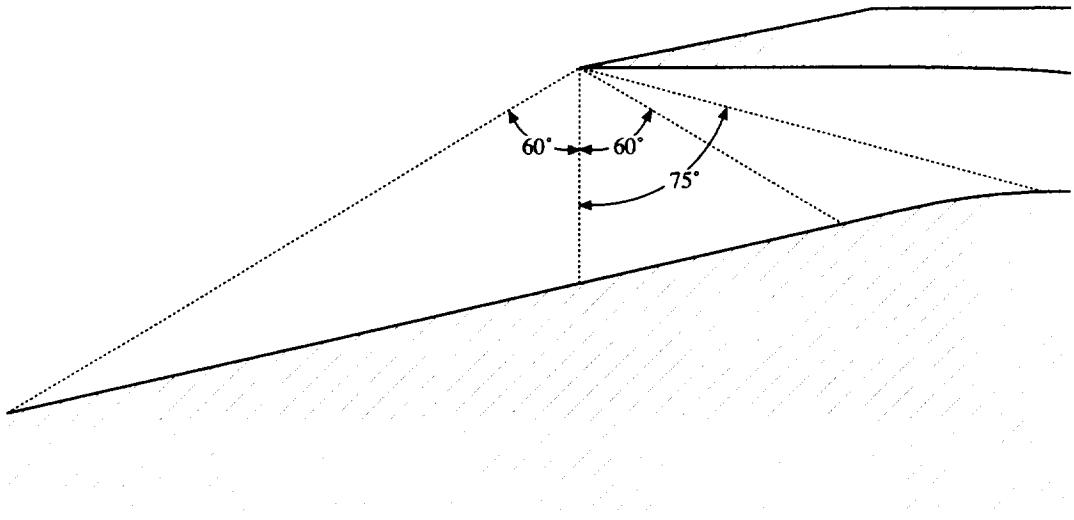

Figure 7. End-wall configurations

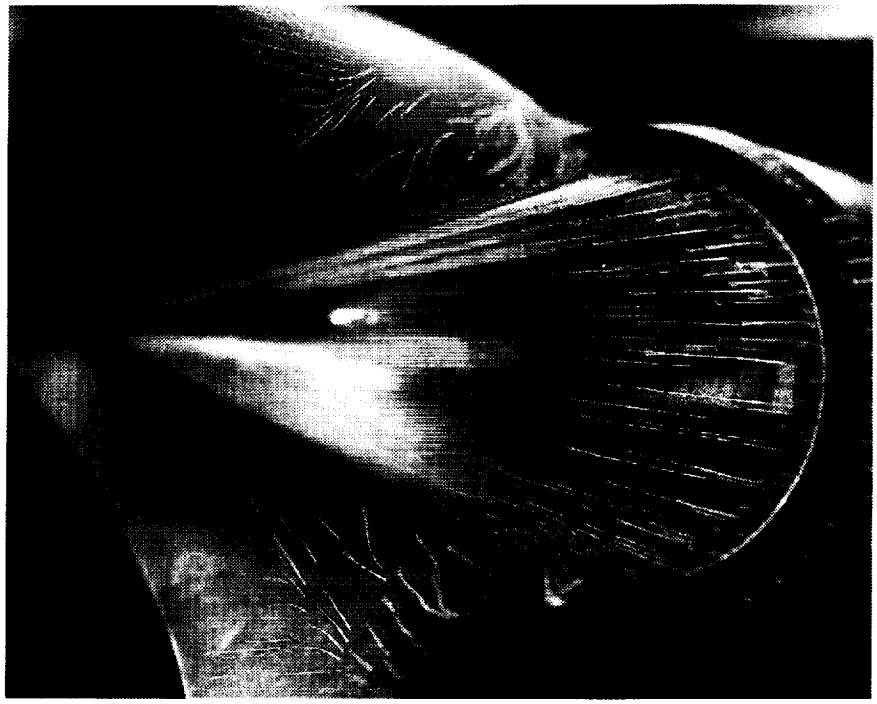

a. overview

b. shock-wave boundary-layer interaction on 60^0 swept forward endwall

Figure 8. Oil flow visualization

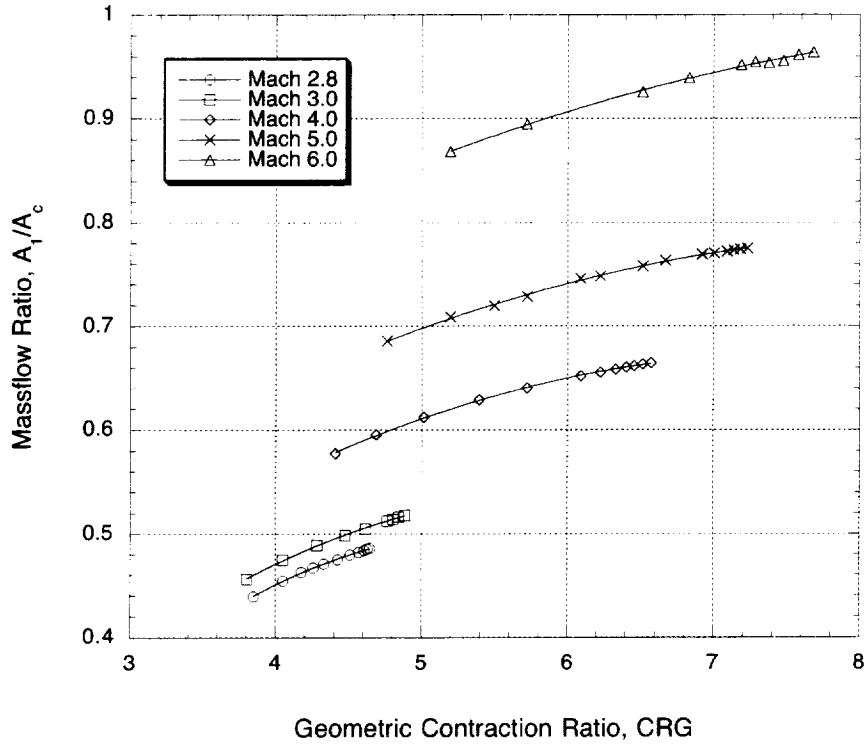

Figure 9. Mass capture for contraction ratio sweeps

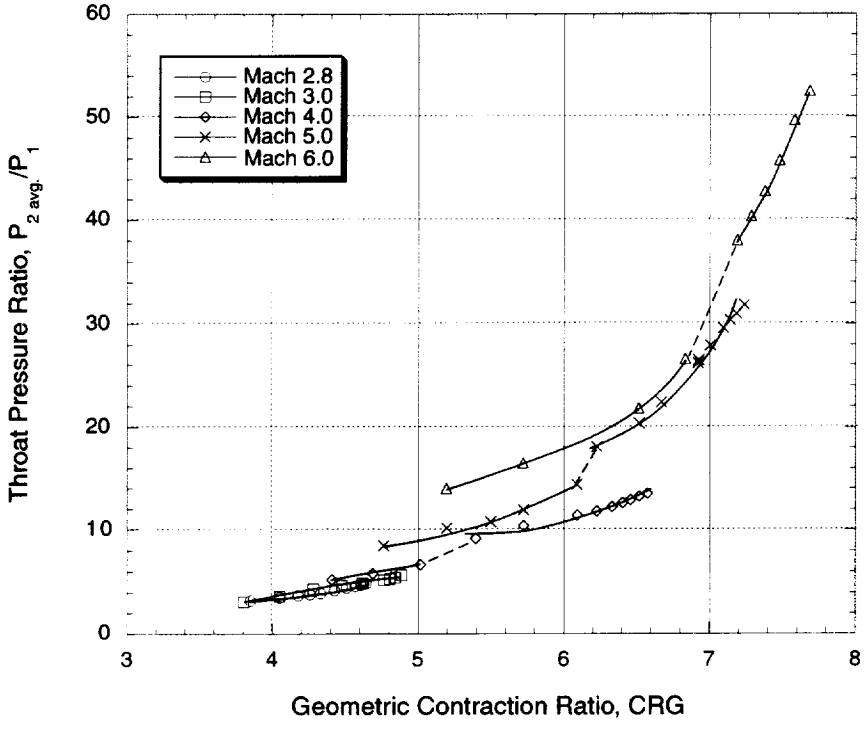

Figure 10. Average throat pressure for contraction ratio sweeps

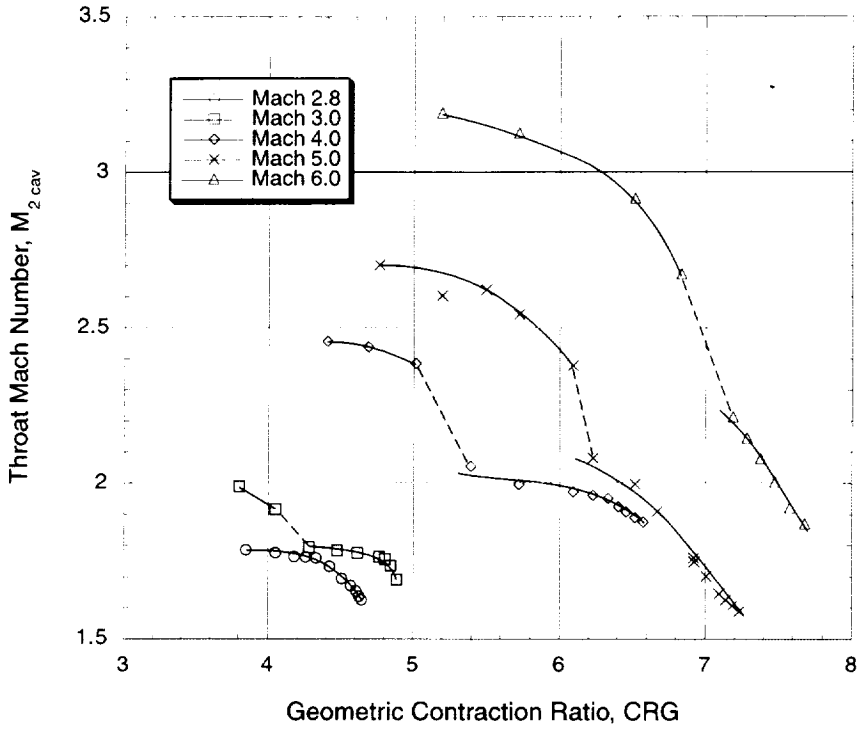

Figure 11. Throat Mach number for contraction ratio sweeps

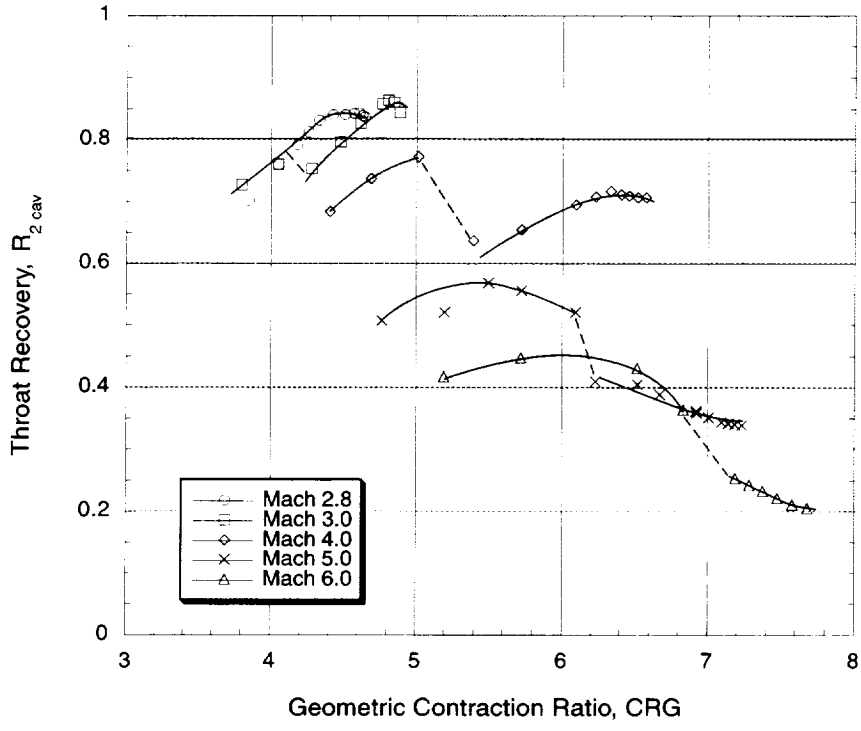

Figure 12. Throat recovery for contraction ratio sweeps

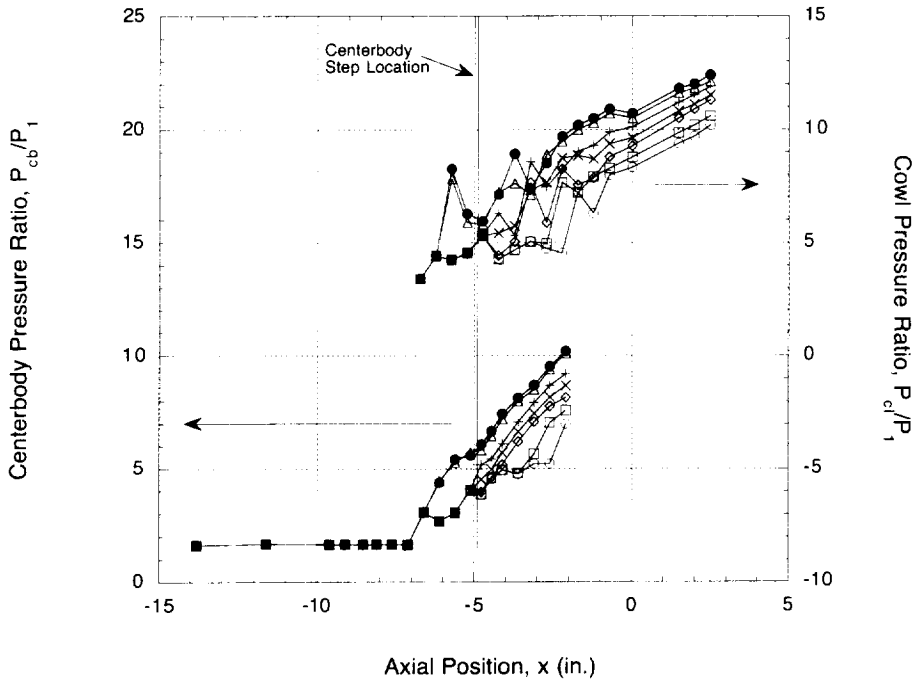

a. Mach 2.8

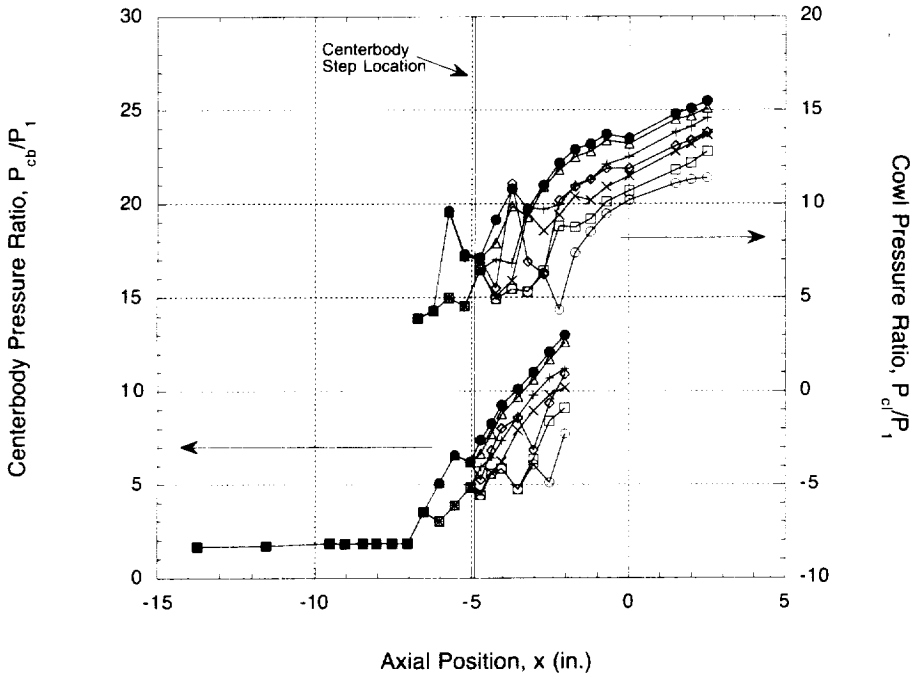

b. Mach 3.0

Figure 13. Pressure distributions on inlet centerline

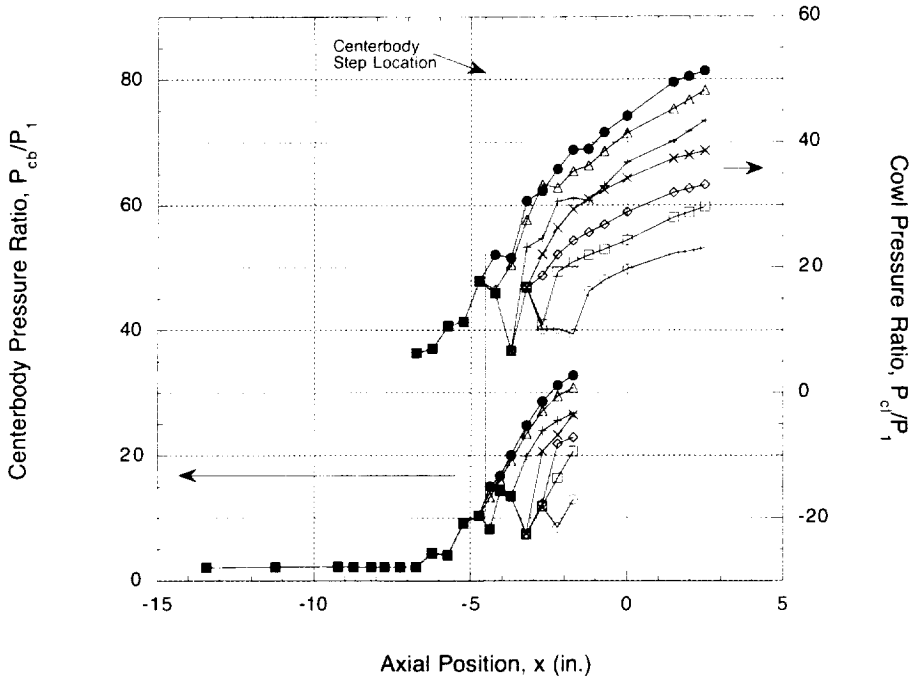

c. Mach 4.0

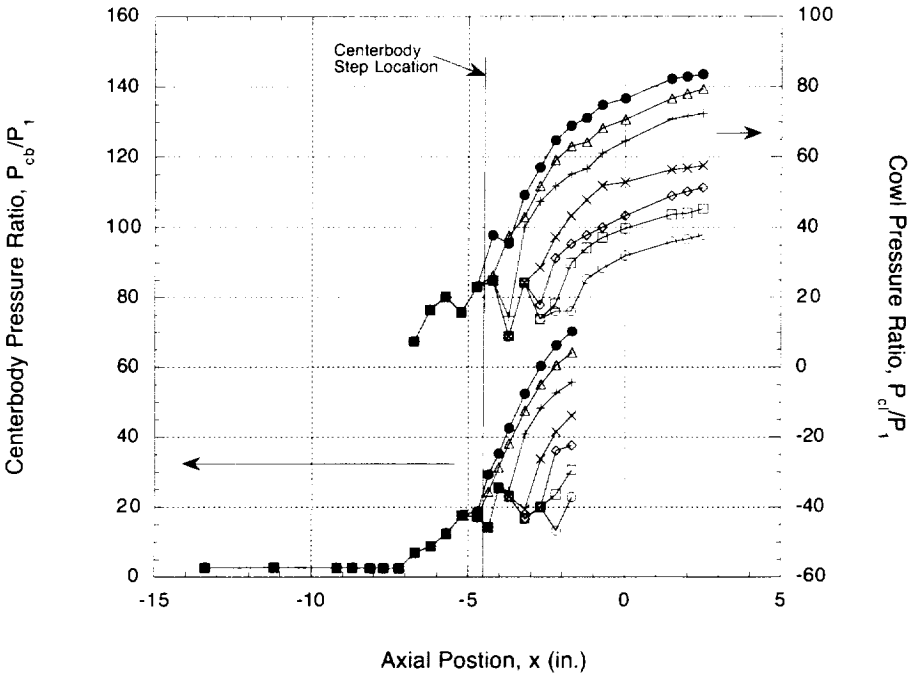

d. Mach 5.0

Figure 13. continued

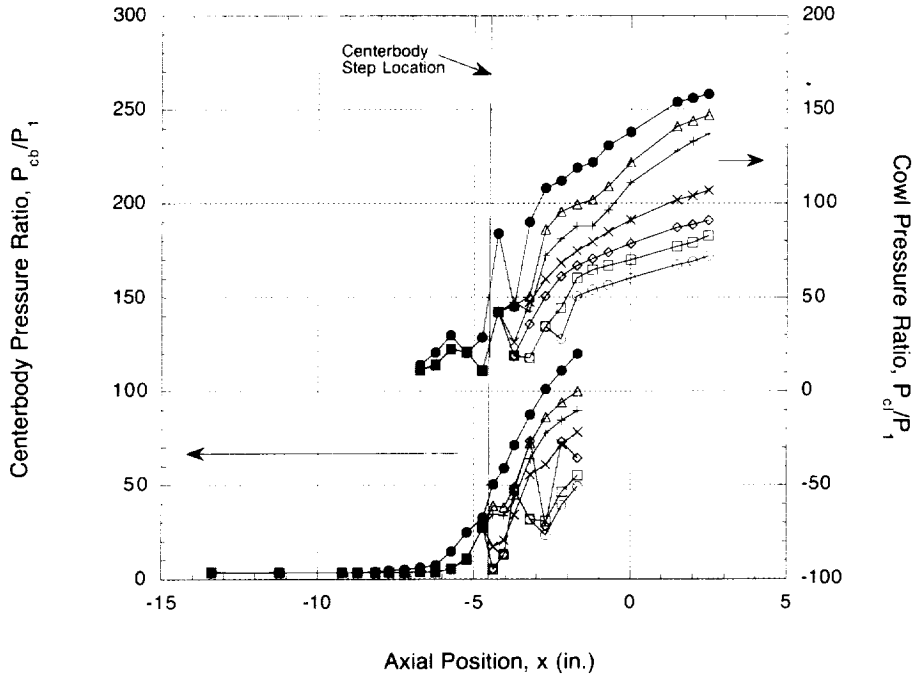

e. Mach 6.0

Figure 13. continued

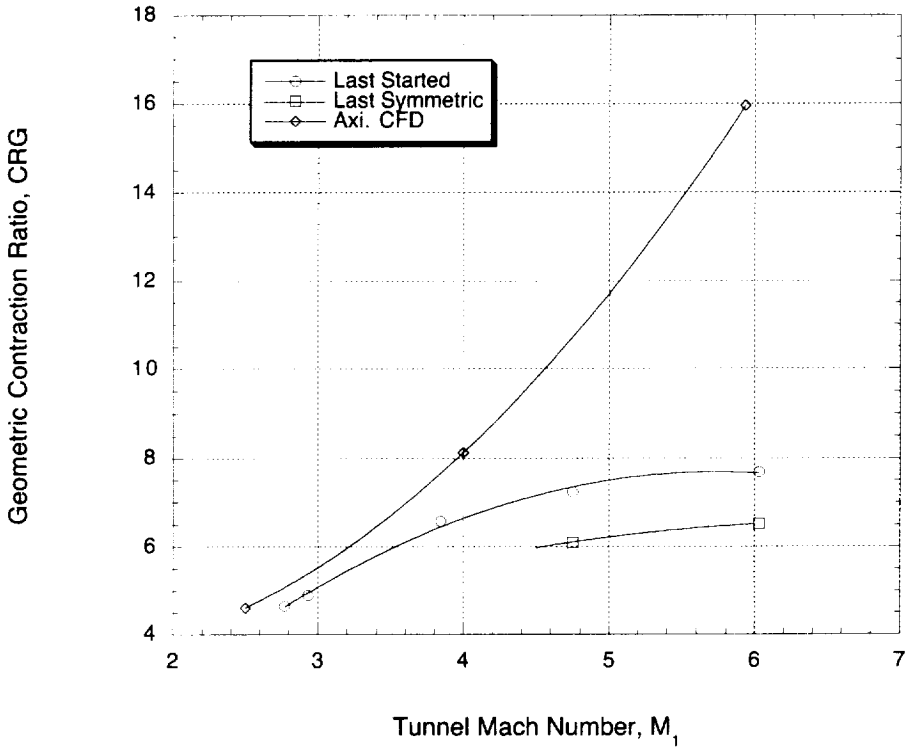

Figure 14. Contraction ratio

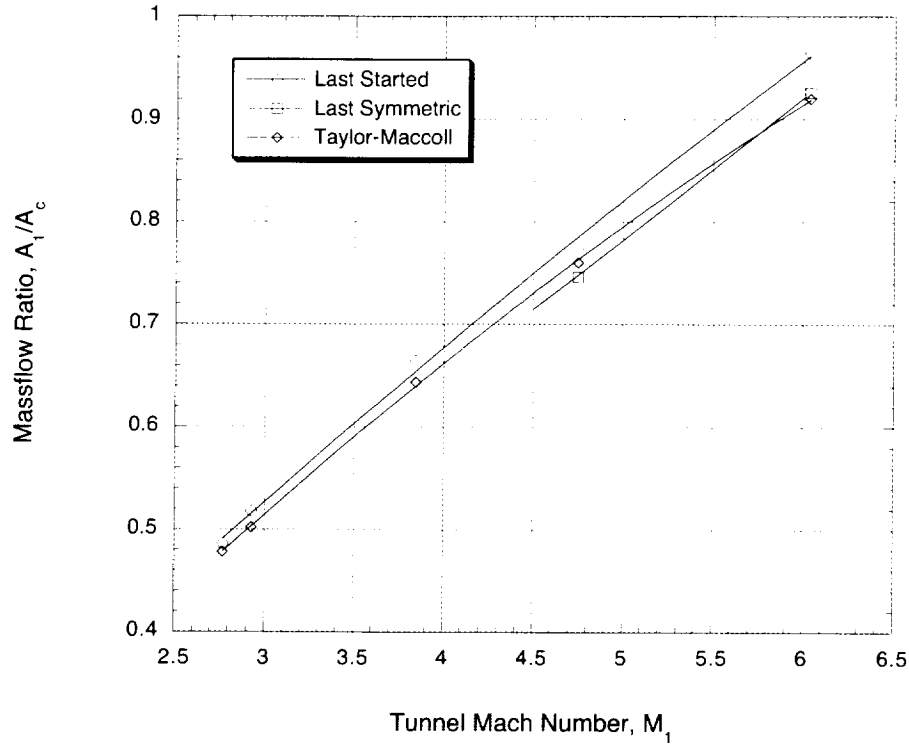

Figure 15. Massflow ratio

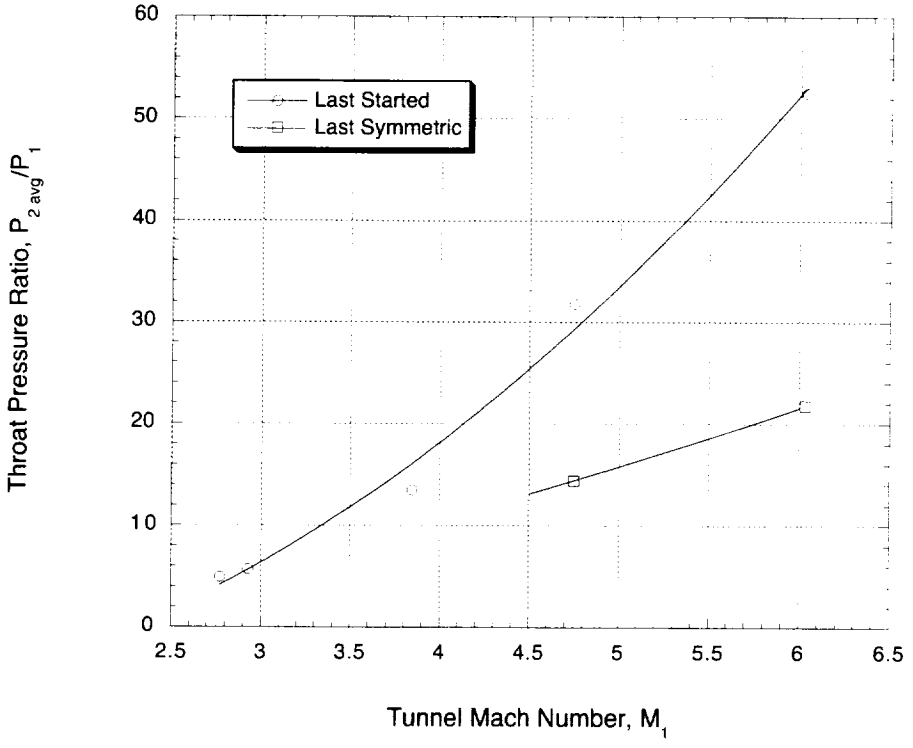

Figure 16. Average throat pressure

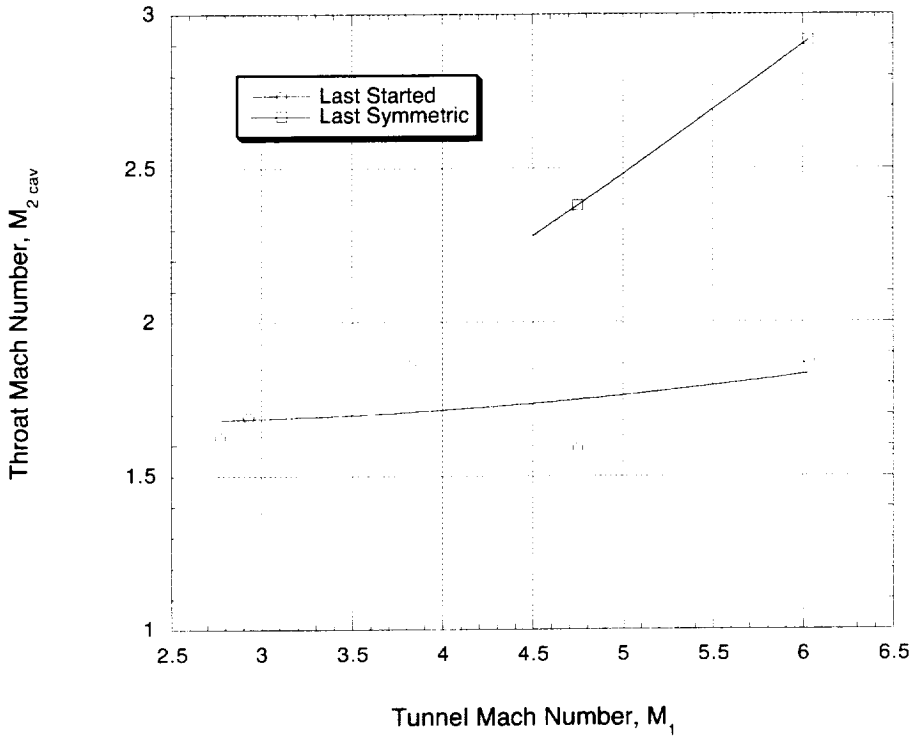

Figure 17. Throat Mach number

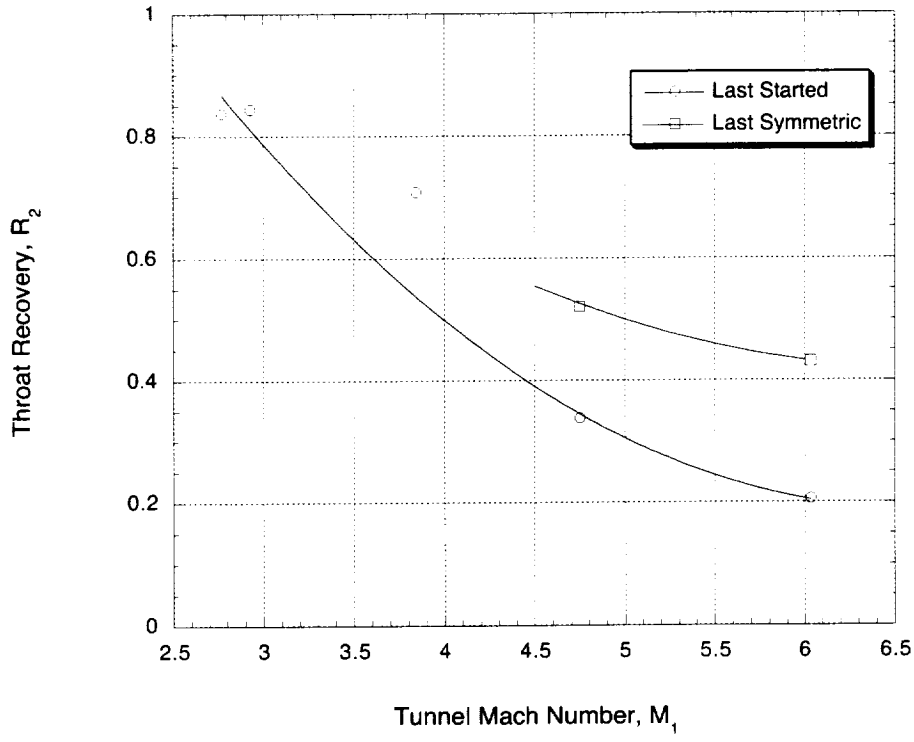

Figure 18. Throat recovery

REPORT DOCUMENTATION PAGE

Form Approved
OMB No. 0704-0188

1. AGENCY USE ONLY (*Leave blank*)	2. REPORT DATE	3. REPORT TYPE AND DATES COVERED
	February 2001	Technical Memorandum

4. TITLE AND SUBTITLE

Supersonic Wind Tunnel Tests of a Half-Axisymmetric 12°-Spike Inlet to a Rocket-Based Combined-Cycle Propulsion System

5. FUNDING NUMBERS

WU–523–61–33–00

6. AUTHOR(S)

J.R. DeBonis and C.J. Trefny

7. PERFORMING ORGANIZATION NAME(S) AND ADDRESS(ES)

National Aeronautics and Space Administration
John H. Glenn Research Center at Lewis Field
Cleveland, Ohio 44135–3191

8. PERFORMING ORGANIZATION REPORT NUMBER

E–12533

9. SPONSORING/MONITORING AGENCY NAME(S) AND ADDRESS(ES)

National Aeronautics and Space Administration
Washington, DC 20546–0001

10. SPONSORING/MONITORING AGENCY REPORT NUMBER

NASA TM—2001-210567

11. SUPPLEMENTARY NOTES

Prepared for the 37th Combustion Subcommittee, 25th Airbreathing Propulsion Subcommittee, and 19th Propulsion Systems Hazards Subcommittee Joint Meeting sponsored by the Joint Army-Navy-Air Force Interagency Propulsion Committee, Monterey, California, November 13–17, 2000. Responsible person, James R. DeBonis, organization code 5860, 216–433–6581.

12a. DISTRIBUTION/AVAILABILITY STATEMENT

Unclassified - Unlimited
Subject Category: 07 Distribution: Nonstandard

Available electronically at http://gltrs.grc.nasa.gov/GLTRS

This publication is available from the NASA Center for AeroSpace Information, 301–621–0390.

12b. DISTRIBUTION CODE

13. ABSTRACT ***(Maximum 200 words)***

Results of an isolated inlet test for NASA's GTX air-breathing launch vehicle concept are presented. The GTX is a Vertical Take-off/Horizontal Landing reusable single-stage-to-orbit system powered by a rocket-based combined-cycle propulsion system. Tests were conducted in the NASA Glenn 1- by 1-Foot Supersonic Wind Tunnel during two entries in October 1998 and February 1999. Tests were run from Mach 2.8 to 6. Integrated performance parameters and static pressure distributions are reported. The maximum contraction ratios achieved in the tests were lower than predicted by axisymmetric Reynolds-averaged Navier-Stokes computational fluid dynamics (CFD). At Mach 6, the maximum contraction ratio was roughly one-half of the CFD value of 16. The addition of either boundary-layer trip strips or vortex generators had a negligible effect on the maximum contraction ratio. A shock boundary-layer interaction was also evident on the end-walls that terminate the annular flowpath cross section. Cut-back end-walls, designed to reduce the boundary-layer growth upstream of the shock and minimize the interaction, also had negligible effect on the maximum contraction ratio. Both the excessive turning of low-momentum corner flows and local over-contraction due to asymmetric end-walls were identified as possible reasons for the discrepancy between the CFD predictions and the experiment. It is recommended that the centerbody spike and throat angles be reduced in order to lessen the induced pressure rise. The addition of a step on the cowl surface, and planar end-walls more closely approximating a plane of symmetry are also recommended. Provisions for end-wall boundary-layer bleed should be incorporated.

14. SUBJECT TERMS

Hypersonic inlets; Integral rocket ramjets; Air breathing engines

15. NUMBER OF PAGES

24

16. PRICE CODE

A03

17. SECURITY CLASSIFICATION OF REPORT	18. SECURITY CLASSIFICATION OF THIS PAGE	19. SECURITY CLASSIFICATION OF ABSTRACT	20. LIMITATION OF ABSTRACT
Unclassified	Unclassified	Unclassified	